Vorticity scattering measurements in a superfluid inertial round jet

Davide Durì, Julien Salort, Pantxo Diribarne, Philippe-Emmanuel Roche, Christophe Baudet

Vorticity scattering measurements in a superfluid inertial round jet

D. Duri[1,2], J. Salort[3], P. Diribarne[2], P.-E. Roche[3] and C. Baudet[1]

[1] UJF-Grenoble 1 / Grenoble-INP / CNRS, LEGI UMR 5519, Grenoble, F-38041, France
[2] SBT, UMR-E CEA/UJF-Grenoble 1, INAC, Grenoble, F-38054, France
[3] Institut Néel, CNRS/UJF, BP166, F-38042 Grenoble Cedex 9, France

E-mail: `davide.duri@cea.fr`

Abstract. The aim of this proceeding paper is twofold. First, we present a newly developed cryogenic testing facility where a steady high Reynolds liquid helium inertial round jet flow is generated allowing to address classical turbulence issues, such as statistical intermittency, and quantum turbulence when the facility is operating in superfluid helium. Secondly we present the first spatial Fourier vorticity modes measurements made both above and below the superfluid transition at different nozzle velocities. These preliminary results were obtained by probing the vorticity flow-field with the ultrasonic scattering technique.

1. Introduction

Helium at cryogenic temperatures is a powerful and versatile working fluid since its physical properties allow to perform a wide range of experiments in turbulence (Donnelly, 1999; Castaing *et al.*, 2000; Niemela & Sreenivasan, 2006). A long standing problem in classical fully developed turbulence is, for instance, the statistical intermittency (Frisch, 1995) and a better understanding of this phenomenon requires, from an experimental point of view, to increase the range of scales involved in the cascade process, from the injection scale L down to the Kolmogorov dissipative scale $\eta = L\mathrm{Re}_L{}^{(-3/4)}$ to obtain a better estimation of the statistical properties of the turbulence in the inertial range where power law scalings are expected. This could be accomplished by increasing the Reynolds number $\mathrm{Re}_L = UL/\nu$, where U is a characteristic fluid velocity, taking advantage of the the low kinematic viscosity, ν, of the gaseous phase (e.g. $3.2 \times 10^{-8}\mathrm{m}^2/\mathrm{s}$ at 5.5 K and 2.8×10^5 Pa) and the liquid phase He I (e.g. $1.8 \times 10^{-8}\mathrm{m}^2/\mathrm{s}$ at 2.2 K and saturated vapor pressure). A carefully controlled steady flow with a Reynolds number varying from 10^4 to 10^7 can be achieved in a relatively compact testing facility, as demonstrated in Chanal *et al.* (2000) and Pietropinto *et al.* (2003). Working with liquid helium also allows to address the problem of the quantum turbulence at high Reynolds number (Maurer & Tabeling, 1998). The liquid phase He I has classical N-S fluid properties but below $T_\lambda \approx 2.17$ K a phase transition, called superfluid transition, occurs and a new liquid phase, called He II, appears. This phase is described by the two-fluids model (Landau & Lifshitz, 1987) and consists of two mutually intricated components: the viscous and the superfluid components. The former is characterized by a finite viscosity, a density ρ_n and a velocity v_n and behaves like a N-S newtonian fluid while the latter, with density ρ_s and velocity v_s, has zero viscosity. The vorticity of the superfluid component allows only the presence of discrete vortex filaments, with quantized circulation,

forming tangles (Vinen & Niemela, 2002). The relative motion of these tangles with respect to the normal component introduces a friction force that should be taken into account as an additional dissipation mechanism whose effects on the developed turbulence energy spectrum are subject of experimental and theoretical studies.

In this paper we first present a newly developed and tested cryogenic wind tunnel facility where a steady high Reynolds liquid He I or He II submerged round jet flow is generated allowing to address classical and quantum restricted turbulence issues in the same flow geometry. Secondly we present the first spatial Fourier vorticity modes measurements made in both He I and He II phases. These preliminary results were obtained by probing the vorticity flow-field with the ultrasonic scattering technique (Lund & Rojas, 1989; Baudet *et al.*, 1991).

2. Experimental facility

The cryogenic wind tunnel testing facility (figure 1(a)) consists of a pressurized closed circuit of structurally integrated components: a centrifugal pump, powered by an external DC motor, a Venturi flowmeter, a coiled heat-exchanger, a settling chamber and the cylindrical testing chamber. The entire wind tunnel structure is immersed in a liquid helium bath (outer bath) at saturated vapor pressure. This inverted "Claudet" bath configuration allows a fine tuning of the wind tunnel working fluid temperature from 4.2 to 1.7 K by reducing the outer bath pressure with an auxiliary vacuum pumping unit. The circuit pressure is controlled independently and can be adjusted above the helium critical pressure ($P_{crit} \approx 2.28 \times 10^5$ Pa) to avoid the impeller cavitation. Typical working pressure ranges from 2.5 to $3{\times}10^5$ Pa. The subcooled round jet develops from a $D = 8$ mm diameter brass conical nozzle inside a cylindrical chamber 25 D in diameter and 60 D in length where the measurement instruments are installed. In order to prevent the onset of non stationary phenomena such as the jet flapping or precessing due to the lateral and longitudinal confinement a stabilizing metallic grid is placed at $40D$ downstream the nozzle exit(Nathan *et al.*, 1998; Chanal *et al.*, 2000). We were able to sustain stable experimental conditions with a constant Reynolds number, $\mathrm{Re}_D = \rho D V_j/\eta$ of $\approx 4{\times}10^6$ at a fixed temperatures comprised between 2.3 and 2.0 K. The Reynolds number is calculated considering the nozzle exit velocity V_j and, in the He II case, the total density $\rho = \rho_n + \rho_s$. Under these conditions the maximum superfluid fraction, $\rho_s/\rho \approx 40\%$.

3. Instruments

3.1. Vorticity scattering measurements

The time evolution of a well defined spatial Fourier mode of the vorticity field $\vec{\omega} = \vec{\nabla} \times \vec{V}$ can be probed by measuring the amplitude and phase modulation of a plane acoustic wave being scattered by the spatial turbulent vorticity fluctuation, as postulated theoretically in Lund & Rojas (1989) and demonstrated experimentally in Baudet *et al.* (1991). A typical acoustic scattering experiment adopts a bistatic configuration (see Poulain *et al.*, 2004) of transducers to send a monochromatic ultrasound carrier wave having frequency ν_0 and pressure $p_{inc}(t)$ towards the turbulent flow-field. The recorded scattered complex amplitude:

$$p_{scatt}(t) \propto \tilde{\Omega}_\perp(\vec{k}, t) p_{inc}(t), \tag{1}$$

is modulated by the Fourier spatial transform of the vorticity component normal to the scattering plane:

$$\tilde{\Omega}_\perp(\vec{k}, t) = \iiint_{\mathcal{V}_{scatt}} \Omega_\perp(\vec{x}, t) \exp^{-i\vec{k}\cdot\vec{x}} \, \mathrm{d}^3x. \tag{2}$$

It should be stressed out that this technique is non local in the physical space since $\mathcal{V}_{scatt}$ is the measurement volume defined by the intersection of the emitting and receiving acoustic

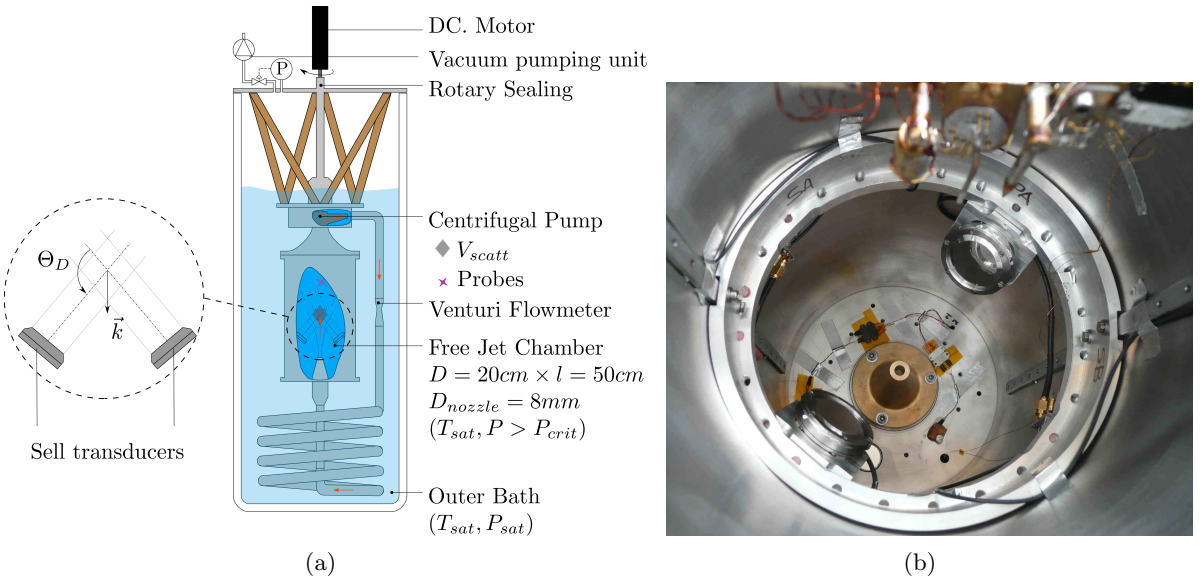

Figure 1. Schematic drawing 1(a) of the cryogenic wind tunnel testing facility (not in scale). The enlarged view shows the ultrasound acoustic scattering set-up geometry. 1(b) shows a photograph of the transducers and the nozzle, taken from the top of the test chamber.

transducers main lobes. The spatial Fourier wave vector $\vec{k}$ is selected by means of the scattering angle Θ_d, defined by the relative orientation of the transducers in the experimental set-up, and the carrier frequency ν_0:

$$\vec{k} = \frac{4\pi}{c}\nu_0 \sin\left(\frac{\Theta_d}{2}\right)\vec{x}, \tag{3}$$

with c denoting the liquid helium sound speed in He I and sometimes called "first sound" in He II.

3.2. Measurement set-up

We used two homemade electroacoustic transducers (Sell type), 32 mm in diameter, positioned inside the cryogenic wind tunnel testing chamber $\simeq$ 160 mm apart with a scattering angle Θ_d of 120°. The geometric center of the measurement volume $\mathcal{V}_{scatt}$ is located on the jet axis at $x/D \approx 30$ downstream and its longitudinal length scale L is of the order of the expected longitudinal integral length scale of the flow $L_{int} \approx 15$ mm. The acoustic arrangement (figure 1(b)), facing the exit section of the testing chamber and resulting in a selected wave vector having opposite direction with respect to the mean flow velocity vector, has been selected to reduce the possibility of perturbing the jet. The internal oscillator of a Signal Recovery 7280-DSP lock-in amplifier is used to drive, after being amplified by a NF HSA-4101 high speed amplifier, the emitting ultrasound transducer with a sine wave signal at frequency ν_0. Both transducers are polarized with a DC bias of 300 V. The electric charge signal, proportional to the scattered pressure received by the second transducer, is converted to a voltage signal using a Stanford Research SR570 charge amplifier. Before being narrow-band demodulated by the lock-in the signal is band-pass filtered (usually ±10 kHz around ν_0) by a NF FV-628B filter bank (flat bandpass, rolloff 24 dB/oct). The time evolution of $\tilde{\Omega}_\perp(\vec{k}, t)$ is recovered as a complex signal $z(t) = X(t) + \mathrm{i}Y(t)$, where $X(t)$ and $Y(t)$ are, respectively, the in-phase and the in-quadrature lock-in output signals, and recorded using a National Instruments PXI-4462, 24 bits, 4 channel data acquisition module running on a Adlink PXI-3920 chassis.

3.3. Stagnation pressure anemometer

We measured the velocity fluctuations by means of a stagnation pressure probe as a diagnostic tool to verify the flow-field characteristics. The probe was positioned downstream at $x/D \approx 35$ and $y/D \approx 1.2$. The detailed description of the measurement electronics and acquisition system can be found in Salort *et al.* (2010).

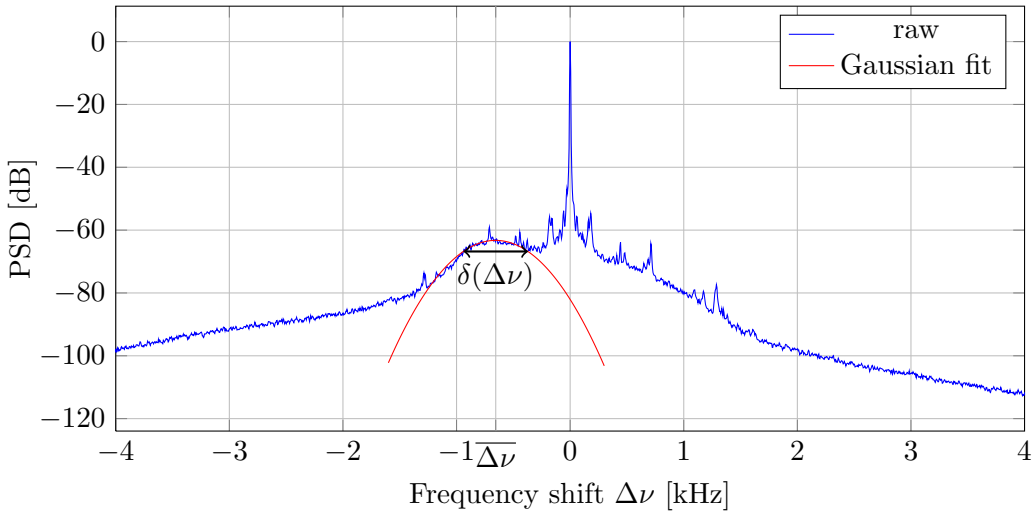

Figure 2. Power spectral density of $z(t)$. The frequency axis is rescaled to represent the frequency shift $\Delta\nu = \nu - \nu_0$.

4. Results

We present the average power spectral density (PSD) of a demodulated scattering complex signal $z(t)$ obtained in He II at $T = 2.0$ K with a Reynolds number of $\simeq 1.8 \times 10^6$ (figure 2). The carrier frequency is $\nu_0 = 292$ kHz determining a wave vector $\vec{k}$ of 7934 rad/m. The signal was sampled at 19531 Hz on 2^{20} data points. The asymmetric scattering power spectrum density is rescaled with respect to the carrier frequency ν_0 and presents several features: a main peak at $\Delta\nu = \nu - \nu = 0$ Hz that is due to secondary diffraction lobes of the transducers that form a direct acoustic path and possible echoes produced within the testing chamber, and a secondary peak centered at $\overline{\Delta\nu} = -655$ Hz. The latter represents the Doppler shift signature (Baudet *et al.*, 1991; Poulain *et al.*, 2004) of the vorticity distribution being advected by the large scale velocity field $\vec{U}$ as:

$$2\pi\Delta\nu = \vec{k} \cdot \vec{U}. \tag{4}$$

The demodulated complex signal $z(t)$ is sensitive to the the direction of the flow and the negative frequency shift confirms the sign dependance on the direction of the scattering vector $\vec{k}$ with respect to the mean flow velocity vector. During the cryogenic wind tunnel calibration we performed a series of acoustic scattering measurements with an increasing jet nozzle velocity, V_j, from 3 to 9 m/s, in both He I and He II, down to a temperature of 2.0 K. The carrier frequency was varied between 140 and 300 kHz, thus leading to a wave vector $\vec{k}$ ranging from 3×10^4 to 1.2×10^5 rad/m. Following the equation 4, we measured the experimental mean advection velocity, named hereafter U_d, by identifying the Doppler shift in each dataset power spectrum. The results are presented in figure 3(a) and show a coherent linear evolution of the measured advection velocity U_d with respect to the increasing mean flow velocity in both He I

and He II. The comparison between U_d and the expected velocity at 30 diameters downstream, represented by the dotted line, shows a fair agreement. As a reference we have considered the classical experimental longitudinal evolution of the mean axial velocity in a round jet (Hussein *et al.*, 1994). The discrepancies have to be taken into account as a consequence of the non-local nature of the measurement technique being affected by the spatial inhomogeneity of the velocity field $\vec{U}$ within the measurement volume. A third feature of the PSD in figure 2 is the broadening

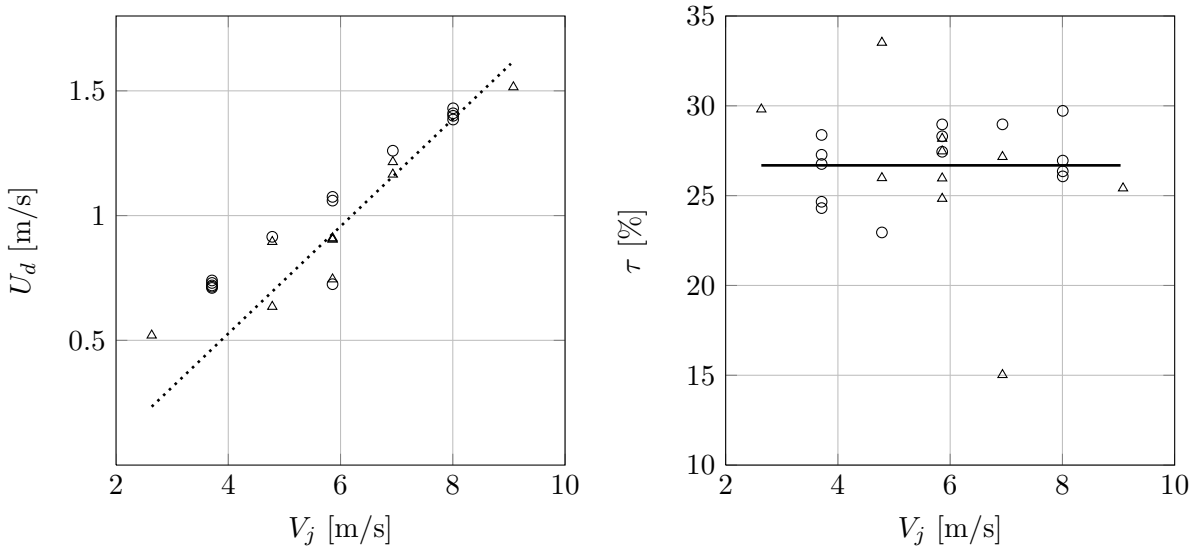

(a) (b)

Figure 3. Measured doppler velocity U_d (3(a)) and turbulence intensity τ (3(b)) as a function of the nozzle velocity V_j at 2.3 K (△) and 2.0 K (○). The dotted line (· · · · · ·) and the solid line (——) represent the expected mean velocity on the jet axis at 30 diameters downstream (Hussein *et al.*, 1994) and the mean of the turbulence intensity, respectively.

of the Doppler peak with respect to its mean frequency. From the equation 4 the broadening, hereafter $\delta(\Delta\nu)$, and the Doppler shift $\Delta\nu$ are related as follows:

$$\frac{\delta(\Delta\nu)}{\Delta\nu} = \frac{\delta\vec{k}\cdot\vec{U}}{\vec{k}\cdot\vec{U}} + \frac{\vec{k}\cdot\delta\vec{U}}{\vec{k}\cdot\vec{U}}. \tag{5}$$

The first term, $\delta\vec{k}\cdot\vec{U}$, represents the contribution of the diffraction effects (Baudet *et al.*, 1991) due to the finite size of the transducers on the wave vector selection, thus affecting the spectral resolution of the apparatus, while $\vec{k}\cdot\delta\vec{U}$ takes into account the fluctuations of the velocity field within the probed volume. According to Poulain *et al.* (2004) $|\delta\vec{k}| \simeq (\mathcal{V}_{scatt})^{-1/3} \simeq 1/L$ is independent of $\vec{k}$ and under this assumption the term $|\delta\vec{k}|/|\vec{k}|$ is in first approximation negligible (Baudet *et al.*, 1991). The broadening $\delta(\Delta\nu)$ can be therefore related to the r.m.s. of the velocity fluctuations as:

$$\sqrt{\overline{u'^2}} = \delta U \propto \delta(\Delta\nu). \tag{6}$$

Following the equations 5 and 6 the broadening gives access to the turbulence intensity of the flow field probed, defined as $\tau = \sigma_d/U_d$. The broadening has been estimated by fitting the Doppler peak with a gaussian distribution having mean $\overline{\Delta\nu}$ and variance $\delta(\Delta\nu)^2$. The results are shown in figure 3(b). We have found an average turbulence level $\tau = 27\% \pm 3\%$, compatible with the results obtained by Wygnanski & Fiedler (1969) in a free jet. The stagnation pressure

probe measurements show that the velocity power spectra are compatible with a Kolmogorov scaling such as in Salort *et al.* (2010).

5. Conclusions

The tests performed in the newly developed and assembled pressurized cryogenic wind tunnel facility demonstrated the possibility of generating an inertial round jet of liquid helium with a Reynolds number up to $\approx 4 \times 10^6$ in He I and He II. We have conducted experiments under reproducible temperature and pressure conditions down to a temperature of 2.0 K. The time evolution of selected spatial Fourier modes of the jet vorticity field at 30 diameters downstream was probed by measuring the scattering of an ultrasonic acoustic (first sound) wave. The Doppler signature of the vorticity structures being advected by the mean flow velocity field and its fluctuations were recovered from the average power spectrum density of the demodulated complex scattering signals at different mean velocities and fluid temperatures. These preliminary results show a satisfactory agreement with respect to the expected evolution of the far field velocity and the mean turbulence level in a self-similar developed round jet. Up to the precision of our present acoustic scattering measurements the Doppler shifts related to advection of the turbulent vorticity fluctuations by the velocity field do not exhibit significant discrepancies between the He I and He II phases. The vorticity measurement by ultrasound scattering is a promising technique that, as shown in this proceeding, can add an alternative insight (see Chevillard *et al.*, 2005) of the developed turbulence at high Reynolds numbers. However more work is still needed to study the dynamics of the vorticity which is expected to have a different behavior in He I than in He II.

Acknowledgments

We thank P. Charvin (SBT) for the technical support that made possible the experiments. This work is supported by the ANR grant No. 09-BLAN-0094, project "SHREK".

References

Baudet, C., Ciliberto, S. & Pinton, J. F. 1991 Spectral analysis of the von kármán flow using ultrasound scattering. *Phys. Rev. Lett.* **67** (2), 193–195.

Castaing, B., Chabaud, B., Hébral, B., Chavanne, X., Chanal, O. & Roche, P.-E. 2000 Cryogenic turbulence experiments. In *Adv. in Turb. VIII* (ed. C. Dopazo), p. 125. Barcelona, France.

Chanal, O., Chabaud, B., Castaing, B. & Hébral, B. 2000 Intermittency in a turbulent low temperature gaseous helium jet. *The European Physical Journal B - Condensed Matter and Complex Systems* **17**, 309–317.

Chevillard, L., Mazellier, N., Poulain, C., Gagne, Y. & Baudet, C. 2005 Statistics of fourier modes of velocity and vorticity in turbulent flows: Intermittency and long-range correlations. *Phys. Rev. Lett.* **95** (20), 200203.

Donnelly, R. J. 1999 Cryogenic fluid dynamics. *J. Physics: Condensed Matter* **11** (40), 7783.

Donnelly, R. J. & Swanson, C. E. 1986 Quantum turbulence. *J. Fluid Mech.* **173**, 387–429.

Elicer-Cortés, J. C. & Baudet, C. 1998 Ultrasound scattering from a turbulent round thermal pure plume. *Exp. Thermal and Fluid Science* **18** (4), 271 – 281.

Frisch, U. 1995 *Turbulence, the legacy of A. N. Kolmogorov*. Cambridge University Press, London.

Hussein, Hussein J., Capp, Steven P. & George, William K. 1994 Velocity measurements in a high-reynolds-number, momentum-conserving, axisymmetric, turbulent jet. *J. of Fluid Mech.* **258**, 31–75.

Landau, L. & Lifshitz, E. 1987 *Fluid Mechanics*, 2nd edn., *Course in Theoretical Physics*, vol. 6. Pergamon Press, London.

Lund, F. & Rojas, C. 1989 Ultrasound as a probe of turbulence. *Physica D: Nonlinear Phenomena* **37** (1-3), 508 – 514.

Maurer, J. & Tabeling, P. 1998 Local investigation of superfluid turbulence. *EPL (Europhysics Letters)* **43** (1), 29.

Nathan, G. J., Hill, S. J. & Luxton, R. E. 1998 An axisymmetric nozzle to generate jet precession. *J. Fluid Mech.* **370**, 347–380.

Niemela, J. & Sreenivasan, K. 2006 The use of cryogenic helium for classical turbulence: Promises and hurdles. *J. Low Temp. Phys.* **143**, 163–212.

Pietropinto, S., Poulain, C., Baudet, C., Castaing, B., Chabaud, B., Gagne, Y., Hébral, B., Ladam, Y., Lebrun, P., Pirotte, O. & Roche, P.-E. 2003 Superconducting instrumentation for high reynolds turbulence experiments with low temperature gaseous helium. *Physica C: Superconductivity* **386**, 512 – 516, in Proc. Intl. Cryogenic Materials Conf. (ICMC 2002).

Poulain, C., Mazellier, N., Gervais, P., Gagne, Y. & Baudet, C. 2004 Spectral vorticity and lagrangian velocity measurements in turbulent jets. *Flow, Turbulence and Combustion* **72**, 245–271.

Salort, J., Baudet, C., Castaing, B., Chabaud, B., Daviaud, F., Didelot, T., Diribarne, P., Dubrulle, B., Gagne, Y., Gauthier, F., Girard, A., Hébral, B., Rousset, B., Thibault, P. & Roche, P.-E. 2010 Turbulent velocity spectra in superfluid flows. *Physics of Fluids* **22** (12), 125102.

Vinen, W. F. & Niemela, J. J. 2002 Quantum turbulence. *J. Low Temp. Phys.* **128**, 167–231.

Wygnanski, I. & Fiedler, H. 1969 Some measurements in the self-preserving jet. *J. Fluid Mech.* **38** (03), 577–612.